Biophysical Variability in the Kuroshio Extension from Altimeter and SeaWiFS

Peter C. Chu and Yu-heng Kuo
Naval Ocean Analysis and Prediction Laboratory
Department of Oceanography
Naval Postgraduate School
Monterey, CA 93943

Abstract— **Ten years (1998-2007) of Sea Level Anomaly (SLA) from multiple satellite altimeters and chlorophyll-*a* concentration from the Sea-viewing Wide Field-of-view Sensor (SeaWiFS) were used to investigate the eddy structure and associated biophysical processes in the Kuroshio Extension (KE) region near 35°N. Seasonal SeaWiFS chlorophyll-*a* concentrations cycles and annual changes of altimeter SLA are derived for the subtropical North Pacific near 35°N and along the KE axis. Spatial structure of SeaWiFS is determined as the deviations from a local seasonal cycle and examined in relation to altimeter eddy structure. In the KE region, SeaWiFS structure is evident during the spring bloom period with a scale around 460 km. Eddy propagation speeds and scales are examined. Cold-core (cyclonic) rings correspond to areas of high SeaWiFS chlorophyll-*a*. Warm-core (anticyclonic) rings relate to areas of low chlorophyll-*a* concentration. SeaWiFS chlorophyll-*a* anomalies and Altimeter SLA structure have an overall negative correlation coefficient of r=−0.36. Swirl currents between eddies redistribute surface chlorophyll concentrations and can spatially bias maximum and minimum concentration levels off eddy center.**

Key Words—**Kuroshio Extension**, **SeaWiFS chlorophyll-*a*, warm-core ring, cold-core ring, negative correlation**

I. INTRODUCTION

The Oyashio flows southwestward along the Kuril Islands and turns eastward from the northern coast of Japan. The Kuroshio flows northward from the tropical area to Tohoku area east of Japan. The Kuroshio turns eastward from the eastern coast of Honshu, Japan, and the strong eastward flow around 35°N is called the Kuroshio Extension (KE), which is the continuation of the warm, northward-flowing waters of the Kuroshio western boundary current, and forms a vigorously meandering boundary between the warm subtropical and cold northern waters of the Pacific. The warm Kuroshio waters encounter the cold dry air masses coming from the
Asian continent, and create intense air sea heat exchanges in the KE region. Solomon [1] discovered a current ring detached from the large quasi-steady Kuroshio meander south of Honshu in May 1977. The ring remained stationary until August, when it recombined with the main Kuroshio to reform a meander distorted in shape and upstream from the original meander. Meanders which separate northward of the KE jet generate anticyclonic (warm-core) eddies and those which separate southward of the KE jet produce cyclonic (cold-core) eddies. The warm-core eddies on the northern side are originated mostly from the area of Sanriku, and the cold-core eddies on the southern side are mainly generated from the area off the Boso Peninsula [2]. A complete life history of cyclonic ring was observed: a southward meander of the KE jet, its pinching-off to form a cyclonic ring, the ring's westward movement, its coalescence with the KE jet [3].

Fig. 1 shows two quasi-stationary meanders with their ridges located at 144°E and 150°E exist along the mean path of the upstream KE [4]. A tight recirculation gyre is located south of the quasi-stationary meanders of the KE jet, and increases the eastward transport of the KE from near 50 Sv to about 130 Sv (where 1 Sv = 10^6 m^3 s^{-1}). Near 159°E, the KE jet encounters the Shatsky Rise where it often bifurcates: the main body of the jet continues eastward, and a secondary branch tends to move northeastward to 40°N where it joins the Subarctic Current [5,6]. With the broadening in its width downstream of 160°E, the KE loses its inertial jet characteristics [7] and rejoins gradually the interior Sverdrup circulation as the North Pacific Current.

Remotely sensed data collected since the late 1970s provides oceanographers with a large volume of information on the state of the surface of the World Ocean. Qiu and Chen [4] analyzed twelve years of sea surface height (SSH) data with its anomaly part [i.e., sea level anomaly (SLA)] from multiple satellite altimeters.

In the KE (mid-latitude western boundary current outflow region), part of SLA measured by the altimeters reflects the seasonally varying surface heat flux that causes expansion or contraction of the water column [8,9]. Qiu and Chen [4] removed these steric height changes from the weekly SLA dataset and investigated the low-frequency changes and the interconnections of the KE jet, its southern recirculation gyre, and their

mesoscale eddy field. Following [4], the axis of the KE jet is defined by the 170-cm SSH contours in the SSH maps, which are consistently located at, or near, the maximum of the latitudinal gradient of SSH (Fig. 2).
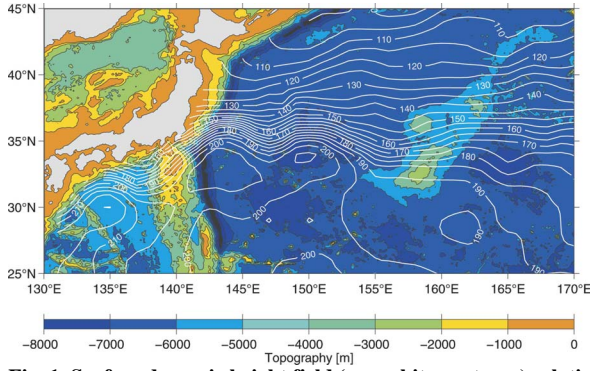
Fig. 1. Surface dynamic height field (cm; white contours) relative to 1000 dbar from Teague et al. [1`0]. Colored map shows the bathymetry based on Smith and Sandwell [11]. Major bathymetric features in the region include the Izu–Ogasawara Ridge along 140°E and the Shatsky Rise around 159°E [4].
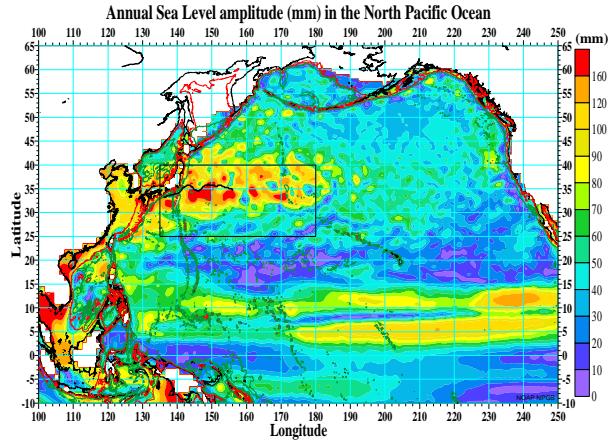
Fig. 2. Annual Sea Level amplitude (mm) in the North Pacific Ocean. The Kuroshio Extension route selected (marked blank) along the 170 cm SSH contour (see Fig. 1), which is associated with large amplitude region.

Many studies have been conducted on the effects of eddies on the transfer and growth of the phytoplankton in the KE counter-part in the North Atlantic (i.e., Gulf Stream). For example, the Gulf Stream warm-core and cold-core rings affect surface phytoplankton distributions via the entrainment of the surrounding water masses around and into the rings [12,13]. Data are provided by sensors collecting information on Sea Surface Temperature (SST), Sea Surface Height (SSH) and the Sea-viewing Wide Field of-view Sensor (SeaWiFS) allowing the analysis of seasonal variations of surface phytoplankton. However, there is lack of such research on the KE region. This study examines the spatial and temporal variability of SeaWiFS chlorophyll-*a* (Chl-*a*) in the KE region in relation to eddy structure. Then, seasonal cycles of Chl-*a* are derived. Finally, spatial structures of eddy and Chl-*a* are identified and compared along the mean KE axis.

II METHODS AND DATA

A. *Sea Level Anomaly*

SLA heights have been measured by the ERS 1/2 and TOPEX/Poseidon satellites from 1 January 1998 to 31 December 2007 at 7-day intervals. Radar altimeters on board the satellite continually transmit signals at high frequencies to Earth and receive reflected signals from the sea surface. The data have been processed according with SLA spatially interpolated to 0.25° in both latitude and longitude. Maps of SLA were derived for the North Pacific to compare with monthly composites of Chl-*a* concentration.

SLA has evident annual cycle and mesoscale structure dominated by eddy or Rossby waves. The annual signal is influenced partially by the ocean circulation and partially by the rise and fall of the sea surface that arises from the expansion and contraction of the ocean due to its heating and cooling with seasonal climatic change. The region of large variance of sea surface height in the North Pacific is along the mean KE jet (represented by 170-cm contour in Fig. 1), where the annual buoyancy and recirculation changes cause a maximum annual elevation change of about ±20 cm (Fig. 2). Since we are interested in elevation structure that correlates with non-seasonal Chl-*a* structure, the annual component and any residual mean elevation removed from the SLA data using the Fourier analysis. Although relatively small in this context, aliasing due to the semi-diurnal tide is also removed. We refer to the resulting data as SLA residuals. The mean KE jet selected is near the maximum annual amplitude of SLA (Fig. 2) and other spectral components tended to show similar distributions of amplitude structure.

Altimeter and Chl-*a* data is also extracted every 0.25° along the mean KE axis (corresponding to 80 stations sampled over a distance of 1820 km; Fig. 3) from January 1998 to December 2007 (10 years period). Temporal variations of sea surface elevation residuals and Chl-*a* along the mean KE axis are plotted on Hovmöller diagrams. An overlapping time window of Chl-*a* anomalies and altimeter residuals is compared.
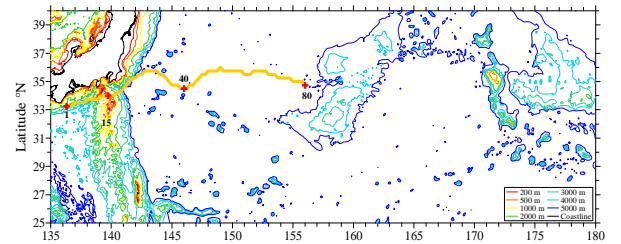
Fig. 3. Topography of the studied area and Kuroshio Extension axis (marked orange) adopted for the present study. Stations positions 1, 15, 40 and 80 are marked.

B. *Chl-a*

Chl-*a* data was obtained from the Goddard Distributed Active Archive Center under the auspices of NASA. Use

of these data is in accordance with the SeaWiFS Research Data User Terms and Conditions Agreement. The SeaDAS software was used to compute Chl-*a* concentration (C_a) from the ratio of radiances measured in band-3 (480–500 nm) and band-5 (545–565 nm) according to the following NASA algorithm,

$$C_a = \exp\left[0.464 - 1.989 \text{Ln}(L_{WM} 490 / L_{WM} 555\right], \qquad (1)$$

and monthly composite Chl-*a* maps for the North Pacific were derived. For deriving the 10 year mean seasonal cycles, the Chl-*a* data is spatially averaged over ±25 km in both latitude and longitude and missing data due to cloud coverage interpolated.

The spring bloom period (taking April 2007 as example) is chosen to determine the influence of eddies on Chl-*a* structure (Fig. 4a). Eddy orbital velocities were determined using the geostrophic relation from SLA residual map (Fig. 4b). To examine such effects, seasonal cycles were removed from the Chl-*a* and SLA data. The Chl-*a* anomalies or residuals were compared to the SLA residuals from January 1998 to December 2007.

III RESULTS

A. Structure of Chl-a and SLA

The Chl-*a* monthly composite for April 2007 shows the spring bloom boundary arbitrarily defined by concentration levels of 0.2 mg m^{-3} Chl-*a* concentration (Fig. 4a). The boundary is not regular but has perturbations due to eddy structure. The North Pacific SLA map for April 2007 (Fig.4b) shows the corresponding mesoscale eddy field. The main open ocean dynamical influence on the Chl-*a* field is either advection or redistribution by eddies as the spring bloom boundary propagates (by growth) northward with a length scale around 480 km.

To identify the association between spatial patterns of eddy and Chl-*a* concentration for the KE extension area (rectangular box in Fig. 4), we re-plot Chl-*a* concentration (in color) and SLA (in contour) in Fig. 5. High SLA values (anticyclonic eddies) are indicated by capital letters (A, B, C, D, E, F, G, H), and low SLA values (cyclonic eddies) are marked as numerical numbers (1, 2, 3, …). Cyclonic (anticyclonic) eddies are co-located with high (low) Chl-a concentration areas.

At Station-1 (136.25°E, 33.25°N) (see Fig. 3), the beginning of the KE jet, Chl-*a* concentration has evident seasonal cycle with a strong spring bloom (March-April) and a weak fall bloom (Fig. 6) with a maximum Chl-*a* concentration of 0.97 mg m^{-3} in April 2000 and minimum Chl-*a* concentration of 0.12 mg m^{-3} in September 2007. Chl-*a* concentrations start to increase in the winter period (after September) as the mixed layer deepens due to winter mixing (with nutrient renewal). The sea surface temperature (SST) on the KE

Observatory mooring site nominally at 32.4°N, 144.6°E (see website: http://www.pmel.noaa.gov/keo/data.html) shows that the bloom maximum occurred near the winter minimum temperature of 18°C (in March). Chl-*a* concentrations are elevated above a mean level from about November to May and structure due to advection or mixing by eddies is evident for these monthly Chl-*a* concentration maps.


(a)

(b)
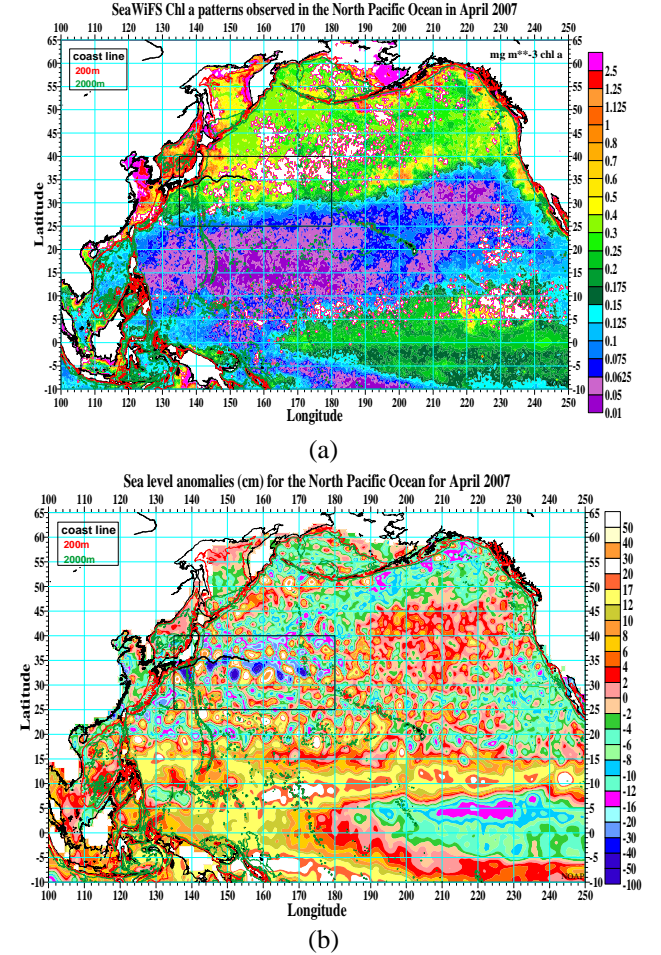
Fig. 4. Satellite observed (a) Chl-*a* concentration (mg/m³) and (b) sea level anomaly (cm) in the North Pacific in April 2007. Kuroshio Extension route is represented by a thick black curve in Fig. 4a.
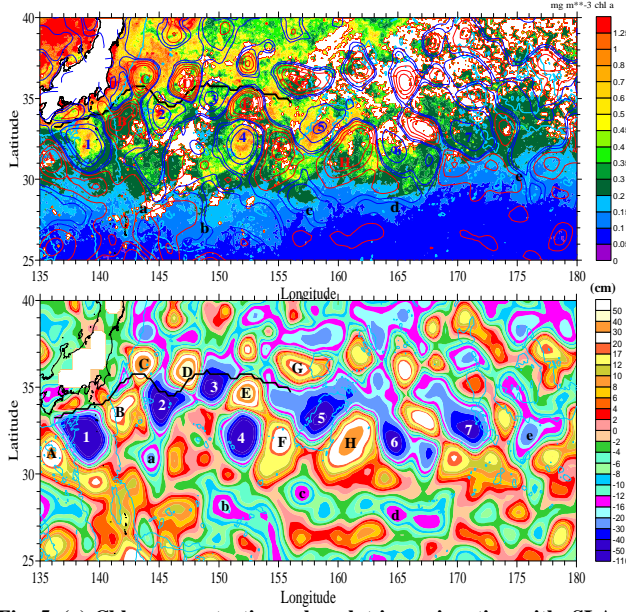
Fig. 5. (a) Chl-*a* concentration color plot in conjunction with SLA (cm) contour, and (b) SLA color plot for the Kuroshio Extension area (25ºN-40ºN, 136ºE-180ºE) in April 2007 . The mean KE jet axis is represented by the thick black curve. Anticyclonic eddies (high SLA) are marked by capital letters (A, B, C, D, E, F, G, H) and cyclonic eddies (Low SLA) are marked by numbers (1, 2, 3, …).
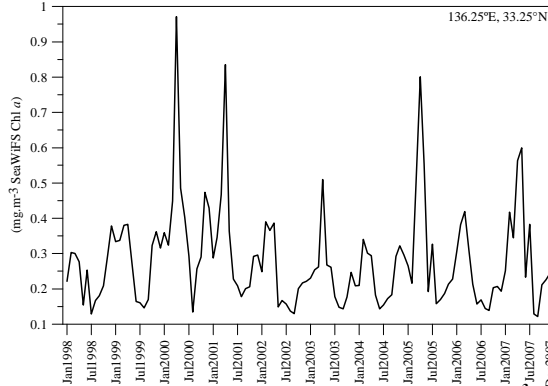
Fig. 6. Temporal variation of Chl-*a* concentration (mg m^{-3} Chl *a*) at 136.25°E, 33.25°N.

B. *Fluctuations of Chl a and SLA along the mean KE jet axis*

Inspection of both SLA and Chl-*a* maps show more intense spatial structure in the KE region. Mean and variance of Chl-*a* concentration (Fig. 7) and variance of SLA (Fig. 8) are calculated at all stations (1-80) nearly 0.25° apart along the mean KE jet axis. There is a significant difference in Chl-*a* concentration between stations 1 and 15 and stations 16 and 80. The mean Chl-*a* concentration is estimated as

$$\overline{x}_{Chla} \pm \sigma = 0.37 \pm 0.02 \text{ mg m}^{-3} \qquad (2)$$

for stations 1 to 15, which is higher than

$$\overline{x}_{Chla} \pm \sigma = 0.28 \pm 0.02 \text{ mg m}^{-3}, \qquad (3)$$

for stations 16 to 80. The difference in Chl-*a* is likely due to the changing properties along the mean KE axis.

Between stations 1 and 15, at the beginning of the KE jet, the waters originated in the Kuroshio and the Oyashio are mixed each other. They interact with the atmosphere and form new water masses. The monthly distribution maps show that high Chl-*a* inflow off Japan coast is most evident in April (see Fig. 5). The SLA shows high fluctuations in variance along the KE axis (Fig. 8),

$$\sigma^2_{SLA} = 870 \pm 460 \text{ cm}^2. \qquad (4)$$
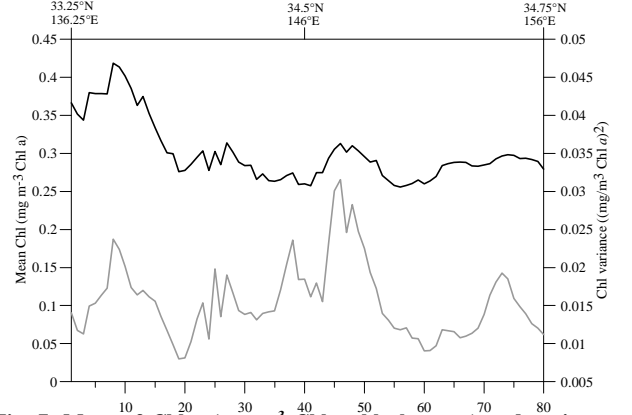
Fig. 7. Mean of Chl-*a* (mg m^{-3} Chl-*a*; black curve) and variance (seasonal cycle removed) of Chl-*a* ([mg m^{-3} Chl *a*]^2; grey curve) along the route of the Kuroshio Extension for a 10 years period (1998-2007).
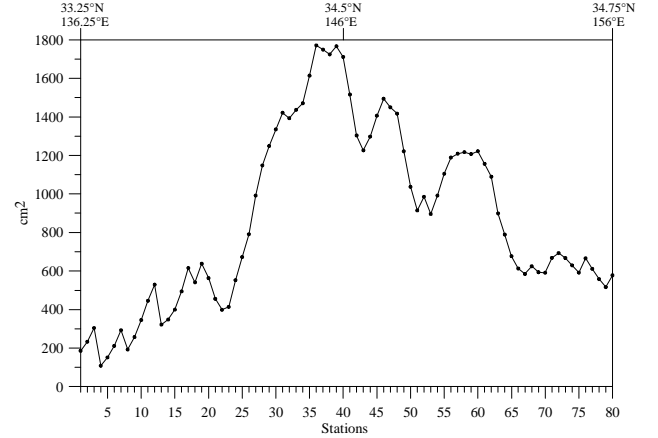
Fig. 8. Variance (annual component removed) of sea level anomalies (cm^2) along the route of the Kuroshio Extension for a 10 years period.

The maximum variance of 1800 cm^2 corresponds to a root mean squared fluctuation of sea level of about ±42 cm on the mean KE jet axis. Variance changes are not correspondence between SLA and Chl-*a* concentration along the KE axis (Figs. 7 and 8). The SLA variance increases generally from 186 cm^2 at Station-1 (33.25ºN, 136.25ºE) to near 1770 cm^2 at Station-36 (34.75ºN, 145ºE). Small SLA variance values might represent a regular pattern of nodes or a meander scale extending 600 km from the position where the KE jet leaves Japanese coast. To seek a relationship between Chl-*a* concentration and SLA variations in the absence of any variance correspondence it will be necessary to take account of phase (time) using the Hovmöller diagrams.

C. Propagation of eddies over time

The SLA residuals have the local annual component removed and the mean value at a point is zero. Intense mesoscale activity, warm-core rings (yellow/red) and cold-core rings (blue), can be identified along the mean KE jet axis (Fig. 9). The propagation of these rings over the time varies according to their location. For example, anticyclonic (A and B) and cyclonic (C) eddies (Fig. 9) moving upstream (westward) in the path of the KE jet have respectively an average speed between 3.05–4.92 km day^{-1} (A and B) and 1.16 km day^{-1} (C). A scale, L, for eddies or rings on the KE jet axis was estimated by measuring the separation distance between positive or negative anomalies along the eastern half of the axis where the anomaly structures were more marked. A separation or anomaly wavelength was determined as

$$L = 460 \pm 65 \text{ km} \tag{5}$$

from Fig. 9, but extended for a 10 year period.
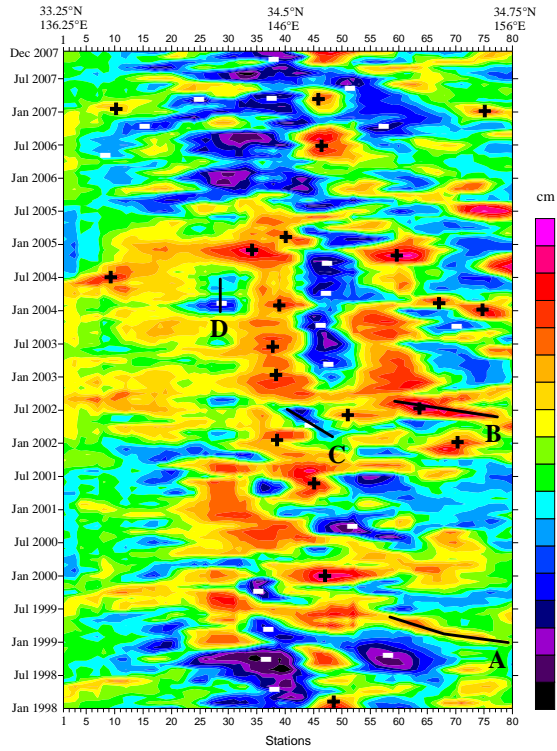
Fig. 9. Hovmöller diagram of SLA residuals along the route of the Kuroshio Extension between January 1998 and December 2007. The altimeter signal is the SLA (cm) with the annual signal removed. Anticyclonic (A, B) and cyclonic (C, D) eddies have been followed in time and space. Negative sign indicates position of a low SLA associated with elevated Chl-*a* anomaly (+ in Fig. 10). Positive sign indicates position of a high SLA associated with lower Chl a anomaly (− in Fig. 10).

3.4. Comparison of SLA and Chl-a concentration along the KE jet axis

Chl-*a* structure in space and time may be masked by a dominant seasonal cycle so the Chl-*a* anomalies or residuals are defined as differences from a mean seasonal cycle. The seasonal cycles obtained for stations 1 to 15 and stations 16 to 80 are shown in Fig. 10. The two blooms occurs, reflecting nutrient limitation in Subtropical Water, with the first bloom (maximum value) in April (0.55 mg m^{-3} Chl-*a*), the second bloom in November (0.43 mg m^{-3} Chl-*a* for stations between 1 and 15, and 0.30 mg m^{-3} Chl-*a* for stations between 16 and 80) and a minimum value in August (0.25 mg m^{-3} Chl-*a* for stations between 1 and 15, and 0.15 mg m^{-3} Chl-*a* for stations between 16 and 80). The spring bloom results from increased light levels and the autumn bloom are a response to nutrient availability due to increased vertical mixing and seasonal thermocline erosion.

Removing the mean Chl-*a* seasonal cycle from the SeaWiFS data for stations 1–80 gives the anomaly time series or Chl-*a* anomalies along the mean KE jet axis (Fig. 11). Warm-core (anticyclonic) rings generally correspond to areas of low Chl-*a* concentration. For example, the anticyclonic eddies marked A and B (Fig.9) corresponds to the low Chl-*a* pattern marked *a* and *b* (Fig. 11). Cold-core (cyclonic) rings generally correspond to high Chl-*a* concentration structure; the cyclonic eddies marked C and D (Fig. 9) corresponds to the high level Chl-*a* pattern marked c and d (Fig. 11). Other lower SLA residuals (marked - in Fig. 9) are associated with higher Chl-*a* values (marked + in Fig. 11) and vice versa. The linear regression equation between Chl-*a* (mg m^{-3}) and SLA (cm) is given by
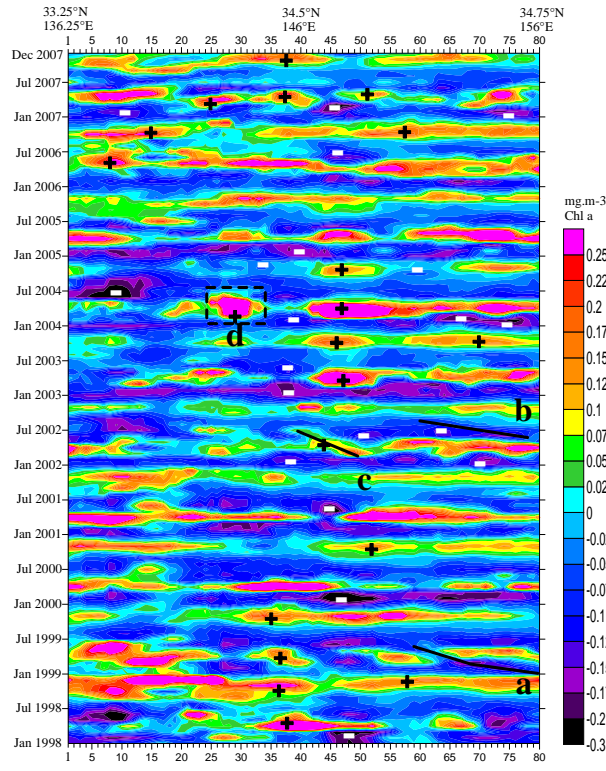
$$\text{Chl-}a = -0.0169\text{SLA}, \tag{6}$$

for Stations 1-15, and

$$\text{Chl-}a = -0.0111\text{SLA}, \tag{7}$$

for Stations 16-80.
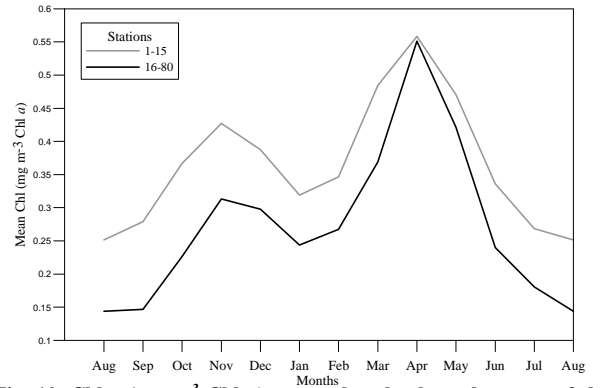
Fig. 10. Chl-*a* (mg m^{-3} Chl *a*) seasonal cycle along the route of the Kuroshio Extension. The results for station 1-15 are in grey and for station 16-80 in black.

Fig. 11. Hovmöller diagram of Chl-*a* residuals along the route of the Kuroshio Extension between January 1998 and December 2007. The Chl-*a* signal is the SeaWiFS Chl-*a* (mg m^{-3}) with the seasonal cycle removed. The high Chl-*a* (c, d) correspond to cyclonic eddies (C, D, Fig. 9) and the low Chl-*a* (a, b) correspond to anticyclonic eddies (A, B, Fig. 9). Positive sign indicates position of elevated Chl-*a* anomaly associated with low SLA (− in Fig. 9). Negative sign indicates position of lower Chl-*a* anomaly associated with high SLA (+ in Fig. 9).
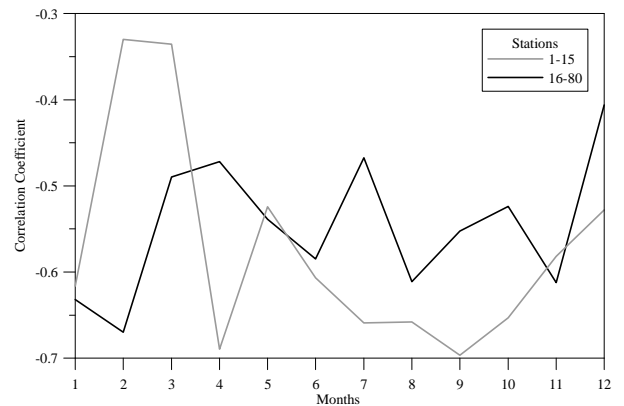
When the relationship between Chl-*a* and SLA residuals is analyzed for the two different water masses sampled along the route, a higher significant correlation is found for the Subtropical Water, for stations 1 and 15 ($r = −0.45$, p<0.001; Fig. 12a) than for the other part of the route, for stations 16 to 80 ($r = −0.35$, p<0.001; Fig. 12b). Values also vary for different months in both water regions (Fig. 13). Such negative correlations have different seasonal variations between two parts along the KE axis. For Stations 1–15, a maximum negative value occurs in September (r ~ −0.70), and a minimum negative value occurs in February (r ~ −0.33). For Stations 16-80, a maximum negative value occurs in February (r ~ −0.67) and a minimum negative value occurs in December (r ~ −0.40). The overall negative correlation for Stations 1-80 is found between Chl-*a* anomalies (Fig. 11) and SLA residuals (Fig. 9) ($r = −0.36$, p<0.001).

The overall correlation coefficient, $r = −0.34$, shows that the chlorophyll scale or anomaly wavelength along the KE jet axis will match the separation scale between SLA residuals or eddies of the same sign. However, the Chl-*a* structure (Fig. 11) was too fragmented for an estimate of scale along the KE jet axis. Instead, a wavelength value was determined from monthly Chl-*a*

concentration maps for occasions when a repeating concentration structure was evident along the KE route. This method gave an independent value of $L = 460±65$ km, based on monthly occurrences when there was a tendency for a repeating structure or oscillation wavelength along the KE route (see Fig. 5, for example). The more regular Chl-*a* structure could be matched (in position and time) with negative SLA anomalies on SLA maps.
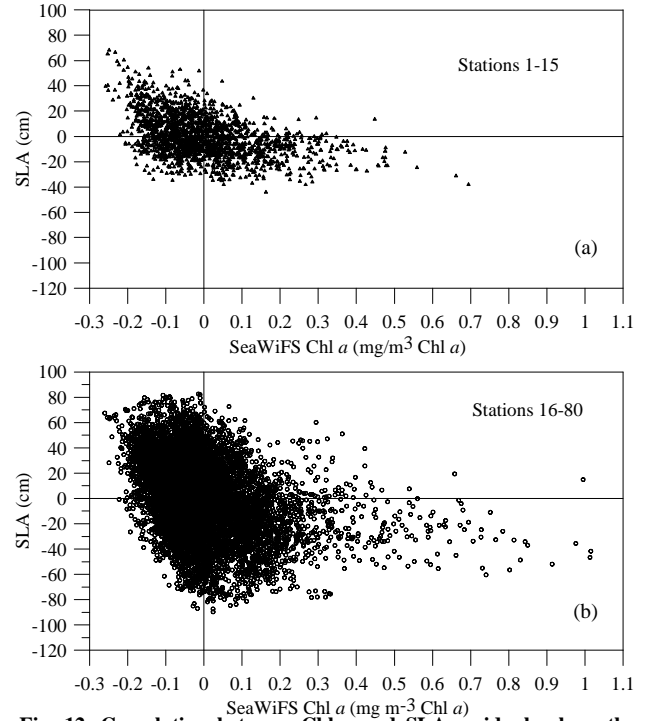
Fig. 12. Correlation between Chl-*a* and SLA residuals along the route of the Kuroshio Extension for (a) stations 1-15 and (b) stations 16-80.

Fig. 13. Monthly correlation coefficient between Chl-*a* anomalies and SLA residuals along the route of the Kuroshio Extension. The results for stations 1-15 are in grey and in black for stations 16-80.

E. Advection of chlorophyll structure by eddies

In the central region of an eddy, the eddy currents move with the eddy and so just turn the chlorophyll structure at near constant radius within the eddy. At external regions, chlorophyll structure can be moved between eddies and so chlorophyll can be mixed across concentration gradients. For eddy currents, to show a significant redistribution of a phytoplankton bloom, the eddy swirl currents must be able to advect phytoplankton concentrations at rates comparable or greater than the propagation rates of concentration structures due to phytoplankton growth dynamics.

The velocity of tangential flow due to eddies can be determined by applying the geostrophic relation to maps of SLA (e.g. Figs. 4b and 5):

$$\frac{v^2}{R} + fv = -g\frac{\Delta\eta}{\Delta n}, \qquad (8)$$

where f is the Coriolis parameter; η is SLA; v is the horizontal tangential swirl velocity; R is the radius of curvature of the eddy; g is the gravitational acceleration; and $\Delta\eta$ is the elevation change over a distance Δn in the normal direction of eddies. Applying Eq. (9) to eddies B/C or E/F (see Fig. 5) and neglecting the curvature term (v^2/R) give maximum speeds between eddies of

$$v \approx \frac{g}{f}\frac{d\eta}{dx} \sim 0.57 \text{ m s}^{-1}. \qquad (9)$$

In the KE region, chlorophyll levels are elevated towards the slope and shelf region and eddy currents could produce curved chlorophyll plume structures of a few hundred kilometers in a several days. For eddies, to be able to produce the chlorophyll structures a, b, c, d and e (see Fig. 5) along the spring bloom frontal boundary, it is necessary to show that the eddy current structure can result in southward flow speeds that are as fast or faster than the northward propagation speed of the chlorophyll structure. For example, consider Chl-*a* plume c on the western side of cyclonic eddy c identified by SLA structure (Fig. 5a).

IV. DISCUSSIONS AND CONCLUSION

In open ocean conditions of the North Pacific (25°N–40°N, 135°W–180°W), SeaWiFS chlorophyll-*a* concentrations are redistributed at the eddy scale by the eddy surface swirl currents. Estimates of eddy surface currents derived from SLA show that chlorophyll structure may be introduced between eddies of opposite sign. The zonal scale for chlorophyll perturbations was determined at ~ 460 km (Fig. 4b) in April near 35°N. The mixing effect of eddies redistributing chlorophyll concentrations will be most marked where there is a gradient in concentrations, the zonal structure of the spring bloom in the North Atlantic in April, for example. Structure with a similar scale (~ 460 km) was observed

for the productive period (November to May) when levels of chlorophyll are elevated.

Leterme and Pingree [13] showed that cyclonic eddies (storms) in the Gulf Stream region could propagate westward at speeds of 3.3 cm s^{-1} near 33°N, could exist for a year or more and could exhibit a zonal ocean color signal (SeaWiFS). They also showed that the surface swirl currents of these more regular or repeating structures are wave-like and so the water with north–south components of flow between positive and negative SLA anomalies does not move westward with the eddy train. Hence, the surface chlorophyll in structures (a, b, c, d, e) is continuously replaced as eddies moving westward, the overall process being one of mixing and exchange.

This passive mixing process for eddies (that carry a pool of surface water with their centers) differs from the surface chlorophyll response usually attributed to plane westward propagating Rossby Waves where changes of internal thermocline structure is believed to force the surface chlorophyll structure [14,15], but is consistent with the recent more general conclusion of Killworth et al. [16]. The east-west components of the eddy motion allow chlorophyll structure to circumscribe an eddy, move between eddies and allow effective transfer when the chlorophyll frontal concentrations or gradients are east-west. The surface Chl-*a* concentration differences between cyclonic and anticyclonic eddy pairs in April and this was believed to be due to the depth of the mixed layer at the start of the spring bloom rather than enhanced growth due to upwelling of nutrient rich water. Later in the season, the depth of seasonal thermocline does not always represent the underlying internal eddy structure being almost level or domed upwards over anticyclonic structure.

The Kuroshio Extension current represents the boundary between Subtropical Water (i.e. with high dynamic heights and lower Chl-*a* levels) and Slope and Subpolar Waters (i.e. with low dynamic heights and elevated Chl-*a* levels) and sea elevation changes or SLA variance levels are a maximum as eddies and meanders cross a mean route. Kuroshio Extension meanders and rings carry different water types across a mean Kuroshio Extension jet position. In this study, a wavelength scale from one cold ring to another along the axis of the Kuroshio Extension jet was determined as 460 km. The rings have shown two distinct types of movement. Both anticyclonic and cyclonic rings have been observed moving upstream. Several warm-core rings can be found moving westward in the Slope Water with speeds between 3.05–4.92 km day^{-1} (3.5 – 5.7 cm s^{-1}). Cold-core rings well separated from the Kuroshio Extension generally move westward at about 1.16 km day^{-1} (1.4 cm s^{-1}).

It is shown that SLA residuals are correlated negatively with chlorophyll residuals with monthly correlation coefficient, r, $-0.7 < r < -0.2$. In general, the positive elevations anomalies are low in chlorophyll with a core of Subtropical Water. Seven anticyclones can be

seen in Fig. 5a. All these positive eddies near the Kuroshio Extension axis have low chlorophyll concentration (labeled A–H, Fig. 5a). Anticyclonic eddies are associated with depressed isotherms with low levels of inorganic nutrients. Along the Kuroshio Extension, lower chlorophyll-*a* residual (marked with − sign, Fig. 11) occur with positive SLA or anticyclonic structure (marked with + sign, Fig. 9). Cyclonic eddies have higher levels of inorganic nutrients, the isotherms are domed upwards and localized upwelling or mixing may introduce new nutrients into the euphotic zone, which could cause higher primary production in their core (Hitchcock et al., 1993; Arístegui et al., 1997). Cold core rings are thus generally higher in Chl-*a* and cyclonic rings marked 1, 2, 3, 4 south of the Kuroshio Extension axis have elevated chlorophyll concentrations (Fig. 5a). The ring or eddy currents may also redistribute the surface Chl-*a* levels, drawing out plumes of locally increased Chl-*a* from regions of higher Chl-*a*. This effect can be seen in some SLA maps and SeaWiFS monthly composites, April 2007 (Fig. 5) for example, where the eddy current structure draws out plumes (Fig. 5, near anticyclonic ring E, or around cyclone 4, for example) and in the Hovmöller diagrams (Figs. 9 and 11). From February to July 2001 and from stations 48 to 40 there is negative SLA anomaly (marked C, Fig. 9). Near the same area and for the same period, a SeaWiFS positive anomaly can be observed in Fig. 11 (labeled c). Overall, the correlation coefficient between SeaWiFS structure and SLA residuals along the selected Kuroshio Extension axis was $r = −0.36$ and the SeaWiFS Chl a spatial variation or meander wavelength was about 460 ± 65 km and equal to the altimeter SLA separation determined between cold-core or warm-core rings along the route.

REFERENCES

[1] Solomon, H., 1978, Detachment and recombination of a current ring with the Kuroshio. Nature, 274, 58-581.

[2] Sun, X., Y. Wang, and Q. Yuan, 1989: The surface path of the Kuroshio Extension's western sector and the eddies on both sides. Chinese Journal of Oceanology and Limnology, 7 (4), 300-311.

[3] Ichikawa, K., and S. Imawaki, 1994: Life history of a cyclonic ring detached from the Kuroshio Extension as seen by the Geosat altimeter. Journal of Geophysical Research, 99 (C8), 15,953-15,966.

[4] Qiu, B., and Chen, S., 2005. Variability of the Kuroshio Extension jet, recirculation gyre and mesoscale eddies on decadal timescales. Journal of Physical Oceanography, 35, 2090-2103.

[5] Mizuno, K., and White, W. B., 1983. Annual and interannual variability in the Kuroshio Current system. Journal of Physical Oceanography, 13, 1847–1867.

[6] Niiler, P. P., Maximenko, N. A., and McWilliams, J. C., 2003. Dynamically balanced absolute sea level of the global ocean derived from near-surface velocity observations, Geophysical Research Letters, 30 (22), 2164, doi:10.1029/2003GL018628.

[7] Joyce, T. M., 1987. Hydrographic sections across the Kuroshio extension at 165°E and 175°W. Deep-Sea Research, 34, 1331–1352.

[8] Stammer, D., 1997. Global characteristics of ocean variability from regional TOPEX/POSEIDON altimeter measurements. Journal of Physical Oceanography, 27, 1743--1769.

[9] Gilson, J., Roemmich, D., Cornuelle, B., and Fu, L.-L., 1998: Relationship of TOPEX/Poseidon altimetric height to steric height and circulation in the North Pacific. Journal of Geophysical Research, 103, 27 947–27 965.

[10] Teague, W. J., M. J. Carron, and P. J. Hogan, 1990. A comparison between the Generalized Digital Environmental Model and Levitus climatologies. Journal of Geophysical Research, 95 (C5), 7167–7183.

[11] Smith, W. H. F., and D. T. Sandwell, 1994. Bathymetric prediction from dense altimetry and sparse shipboard bathymetry. Journal of Geophysical Research, 99, 21803–21824.

[12] Kennelly, M.A., Evans, R.H., Joyce, T.M., 1985. Small scale cyclones on the periphery of a Gulf Stream warm core ring. Journal of Geophysical Research, 95 (C5), 8845–8857.

[13] Leterme, S.C., and R. D. Pingree, 2008 The Gulf Stream, rings and North Atlantic eddy structures from remote sensing (Altimeter and SeaWiFS). Journal of Marine Systems, 69, 177-190.

[14] Uz, B.M., Yoder, J.A., Osychny, V., 2001. Pumping of nutrients to ocean surface waters by the action of propagating planetary waves. Nature 409, 597–600.

[15] Cipollini, P., Cromwell, D., Challenor, P.G., Raffaglio, F., 2001. Rossby waves detected in global ocean color data. Geophysical Research Letters, 28 (2), 323–326.

[16] Killworth, P.D., Cipollini, P., Uz, B.M., Blundell, J.R., 2004. Physical and biological mechanisms for planetary waves observed in satellite-derived chlorophyll. Journal of Geophysical Research, 109 (C07002). doi:10.1029/2003JC001768.